Establishing the relationship between the CERES window and total channel measured radiances for conditions involving deep convective clouds at night

David P. Kratz, Kory J. Priestley, and Richard N. Green
Atmospheric Sciences, NASA Langley Research Center, Hampton, Virginia, USA

Received 16 November 2001; revised 23 January 2002; accepted 30 January 2002; published 6 August 2002.

[1] Characterizing the stability of the Clouds and the Earth's Radiant Energy System (CERES) instrument is critical to obtaining accurate measurements of the radiative energy budget of the Earth's atmosphere-surface system. Composed of three broadband radiometers, the CERES instrument measures radiances in the shortwave (>2000 cm^{-1}), infrared window (835–1250 cm^{-1}), and total regions of the spectrum. Such a choice of radiometers does not allow for a straightforward three channel intercomparison of the CERES measurements. We observed, however, the outgoing infrared spectra of high, cold, optically thick clouds were fairly representative of blackbody emission. This observation suggested a potential relationship between the infrared window radiometer and longwave portion of the total radiometer. Using nighttime measurements made by the CERES instrument aboard the Tropical Rainfall Measuring Mission (TRMM) spacecraft during the first eight months of 1998, we were able to determine a highly correlated relationship between the infrared window and total channel radiances for conditions corresponding to high, cold, optically thick clouds. Comparisons were then made between the measurements and reference line-by-line calculations. From these comparisons, a quantified relationship was derived between the total and window channel radiances which could accurately reproduce one set of results from the other. Such a relationship has allowed for the establishment of a three channel intercomparison for the CERES instrument with an accuracy of ~1% for the case of high, cold, optically thick clouds. An independent relationship based upon the tropical mean is shown to produce results which support the three channel analysis for the deep convective cloud systems. *INDEX TERMS:* 0394 Atmospheric Composition and Structure: Instruments and techniques; 1694 Global Change: Instruments and techniques; 0325 Atmospheric Composition and Structure: Evolution of the atmosphere; 0360 Atmospheric Composition and Structure: Transmission and scattering of radiation; 1640 Global Change: Remote sensing; *KEYWORDS:* CERES, TRMM, radiometer, three-channel-intercomparison, deep-convective-clouds, infrared-window

1. Introduction

[2] Observing Earth's radiant energy budget from space is critical to improving our understanding of Earth's climate system. The Earth Radiation Budget Experiment (ERBE) [*Barkstrom*, 1984; *Barkstrom and Smith*, 1986] was the first initiative to provide simultaneous observations of Earth's radiant energy with identical instruments flying aboard separate satellites. The design of the ERBE instrument was based upon three complementary broadband radiometers which measured the shortwave (>2000 cm^{-1}), longwave (<2000 cm^{-1}), and total regions of the spectrum. Since any two of the ERBE radiometers could be used to simulate the third, a three channel intercomparison, based on redundancy, was available to reveal any changes in the relative sensitivities of the individual radiometers. Such a three channel intercomparison provided confidence in the application of the ERBE measurements over the lifetime of the instrument while mitigating the concern over instrument degradation.

[3] The Clouds and the Earth's Radiant Energy System (CERES) instrument was also designed with three broadband radiometers [*Wielicki et al.*, 1996]. The shortwave and total channels on CERES are similar to those on the ERBE; however, an 835 to 1250 cm^{-1} (8 to 12 μm) infrared window channel replaced the longwave channel. While the window channel has allowed for improved measurements of the radiant energy budget near the Earth's surface and a better evaluation of the climatic impact of changing water vapor abundances, the measurements do not allow for a straightforward ERBE-like three channel intercomparison. Characterizing the stability of the CERES instrument, however, is critical to understanding the measured radiances from CERES. Thus, we have undertaken an investigation to

0148-0227/02/2001JD001170$09.00

determine the conditions under which the CERES window channel measurements can accurately represent the broadband longwave radiances. Since deep convective cloud (DCC) systems are often characterized by nearly blackbody spectra and have cloud tops that extend to altitudes above most of the atmospheric molecular absorption and emission, we hypothesized that, for nighttime case involving such cloud systems, the CERES window and total channel measurements would be highly correlated.

[4] We began our investigation by obtaining CERES nighttime measured radiances from the window and total channel instruments aboard the Tropical Rainfall Measuring Mission (TRMM) spacecraft for the first eight months of 1998. The nighttime total channel radiances are, of course, directly related to broadband longwave radiances. An examination of the CERES data confirmed our hypothesis by revealing a highly correlated linear relationship between the window and total channel measurements for conditions corresponding to deep convective clouds. With the establishment of a relationship between the CERES window and total channel measurements, and thus a relationship between the window channel measurements and broadband longwave radiances, we were able to formulate a three channel intercomparison for the CERES instrument for the case of DCC systems which is analogous to the ERBE three channel intercomparison.

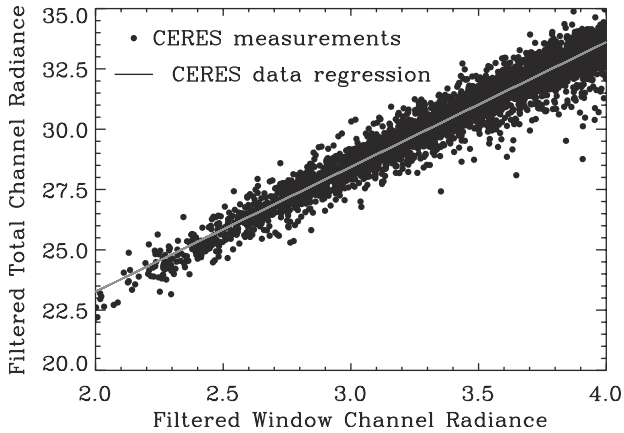

Figure 1. A comparison of the filtered window and filtered total channel radiance measurements (Wm^{-2} sr^{-1}) from the CERES instrument aboard the TRMM spacecraft for the nighttime cases corresponding to the first eight months of 1998. The range in brightness temperatures corresponding to the range in filtered radiances for the window channel is 196K to 217K, and for the filtered total channel is 189K to 217K. The light gray line represents the 8-month mean regression fit of the filtered total channel to the filtered window channel.

2. Observed Nighttime Relationship Between Filtered Window and Filtered Total Channel Radiances

[5] The CERES total channel provides a measure of both the solar energy reflected and the thermal infrared energy emitted by the Earth. For nighttime conditions, where the solar energy is absent, the total channel measures only the broadband longwave energy. For satellite instruments such as ERBE, which have both broadband longwave and total channels, the nighttime measurements allow for an intercomparison that has the potential to uncover any changes in the relative sensitivities of the individual radiometers. The CERES instrument, however, does not have a broadband longwave channel. Instead, the CERES instrument measures radiances in the infrared window region spanning the wave number range from 835 to 1250 cm^{-1} The window region is characterized by relatively weak molecular absorption, and thus for clear sky conditions is fairly transparent. In contrast, the remainder of the thermal infrared is characterized by relatively strong molecular absorption which causes the atmosphere to be fairly opaque irrespective of cloud conditions. Despite this difference, an intercomparison of the nighttime measured nadir radiances from the CERES/TRMM instrument yields a positive correlation between the window and total channel measurements, similar to that observed between the Geostationary Operational Environmental Satellite (GOES) infrared window channels and the ERBE broadband longwave channel [*Minnis et al.*, 1991]. For most atmospheric conditions, however, the regression between the window and total channels produces considerable variance and thus the correlation is not sufficiently precise to allow for accurate simulations of one channel from the other. In contrast, since DCC systems extend to altitudes above much of the atmospheric molecular absorption and emission, we anticipated that most of the energy emitted within the infrared window region and over the broadband longwave should originate from nearly the same altitude regions and thus should be well correlated. Indeed, an examination of the data reveals that for the DCC case there exists a highly correlated linear relationship between the window and total channel measurements (see Figure 1). *Duvel and Raberanto* [2000] have independently noted a similar relationship between the Scanner for Radiation Budget (ScaReB) infrared window (800 to 950 cm^{-1}) and total channel measurements for the case of high, cold clouds (see their Figure 3). Note, the data representing the DCC conditions occur when both the window and total channel radiances are near their minimum values. Thus, the data representing most scene types would be located to the right and above the radiance limits presented in Figure 1.

[6] To understand the observed relationship for DCC, a series of theoretical calculations using the *Kratz and Rose* [1999] line-by-line algorithm in conjunction with the *Minnis et al.* [1993] formulation for cloud optical depths were run to simulate the top-of-atmosphere (TOA) spectral radiances representative of conditions observed by the CERES/TRMM instrument. The accuracy of the *Kratz and Rose* [1999] line-by-line model has been established within the Intercomparison of Radiation Codes in Climate Models (ICRCCM) endeavor [*Ellingson and Fouquart*, 1991] by its very favorable comparison, within established noise limits, with the benchmark line-by-line radiative transfer model (LBLRTM) [*Clough et al.*, 1992; *Clough and Iacono*, 1995] and measurements from the Atmospheric Emitted Radiance Interferometer (AERI) [*Smith et al.*, 1995]. For the present calculations the Kratz and Rose model uses the HITRAN 1996 database [*Rothman et al.*, 1998] and the CKD-2.1 continuum formulation [*Clough*

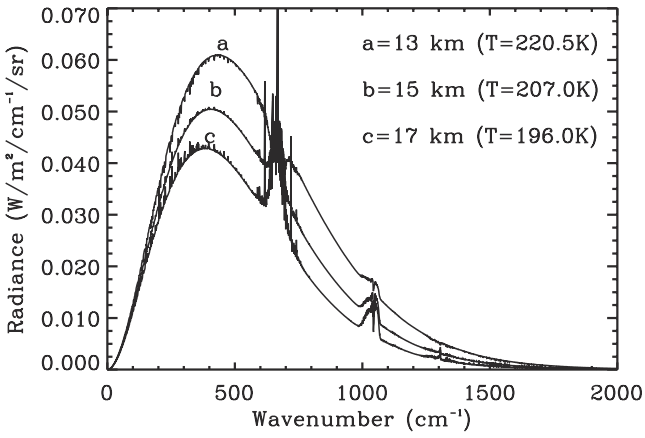

Figure 2. Outgoing spectral radiances for deep convective clouds in the *McClatchey et al.* [1972] tropical atmosphere. The top curve corresponds to the lowest and warmest clouds, while the bottom curve corresponds to the highest and coldest clouds. Note that as the effective emission temperature decreases, the peak of the emission curve shifts noticeably to shorter wave numbers.

et al., 1989]. Observations made with the IRIS instrument aboard Nimbus 4 [*Prabhakara et al.*, 1993] along with the line-by-line calculations have demonstrated that for the DCC case the spectra of the outgoing radiances are fairly representative of optically thick blackbody emission (see Figure 2). Thus, the measured radiances for the DCC case from both the window and total channels should have contribution functions originating from nearly the same altitude regions in the atmosphere. Consequently, the measurements from one channel should be able to be used to reliably predict the measurements from the other. As can be observed from Figure 2, CO_2, O_3 and H_2O affect the outgoing radiances for the DCC case; however, the impact of these trace species upon the contribution function is dominated by the effects of the clouds in the DCC case. In contrast, for clear sky or low cloud conditions, the outgoing TOA radiances measured by the window and total channels frequently provide information associated with different altitude regions in the atmosphere. Thus, for non-DCC conditions, the window and total channels measure radiances originate at different temperatures and pressures; therefore, there is no surprise that one channel cannot accurately simulate the other. Note that the spectral range presented in Figure 2 and in subsequent figures is meant to emphasize the spectral range containing the majority of the thermal infrared energy which occurs within the 0 to 2000 cm^{-1} spectral interval. The present line-by-line calculations, however, have been computed over the 0 to 3000 cm^{-1} range which accounts for over 99.97% of the thermal infrared emission from the Earth's surface.

[7] The functional form of the relationship between the window and broadband longwave radiances was determined by regressing the nighttime window channel measurements against the nighttime total channel data for the same footprints. The functional forms for the total channel radiances, both filtered and unfiltered (i.e., respectively, incorporating and removing the response functions of the CERES instrument), are given in terms of a linear relationship to the filtered window channel:

$$t = a \times w + b \tag{1}$$

where t is the total channel radiance, w is the window channel radiance, and a and b are regression coefficients. To achieve the best fit for our regressions, we sorted the nighttime data by specific geo-physical scene type and limited the geo-location to ±20° latitude. Our analysis was limited to the ±20° latitude range for several significant reasons. First, the bulk of the DCC's occur within the ±20° latitude range. Next, the metric used to identify DCC's (i.e., the window channel brightness temperature) is susceptible to misidentifying snow scenes as DCC's. Finally and most importantly, the ±20° latitude criterion provides consistency with the work of Green and Priestley (The Tropical Mean as a validation parameter for satellite radiances, submitted to *Journal of Atmospheres and Ocean Technology*, 2002) who restricted the tropical mean, which is the average of all the nadir longwave data in the tropics over ocean, to ±20° latitude because the CERES/TRMM instrument has a shallow orbital inclination of 35 degrees. As the inclination decreases, it becomes more difficult to avoid the Sun terminator over the zone and have uniform area sampling. Reducing the width of the tropical zone reduces the longitudinal distance traversed over the zone and allows for more uniform sampling days. In addition, we have limited the regression fits to those cases with integrated filtered window radiances less than 3.76 Wm^{-2} sr^{-1}, which corresponds to a brightness temperature of 215 K. This constraint was imposed to ensure that only DCC cases would be considered. We then created regression fits that

Table 1. Linear Regressions for the Monthly CERES Measurements for the First Eight Months of 1998[a]

Month	a_{uf}	b_{uf}	r^2_{uf}	σ^2_{uf}	a_{ff}	b_{ff}	r^2_{ff}	σ^2_{ff}
January	5.8405	15.216	0.9422	0.4091	5.1346	12.896	0.9426	0.3141
February	5.8857	15.115	0.9552	0.3160	5.1641	12.841	0.9555	0.2419
March	5.8951	15.097	0.9321	0.4363	5.1819	12.793	0.9329	0.3331
April	5.8776	15.130	0.9299	0.4644	5.1616	12.839	0.9305	0.3548
May	6.0022	14.849	0.9500	0.3770	5.2716	12.591	0.9504	0.2886
June	5.7332	15.815	0.9308	0.4295	5.0376	13.431	0.9314	0.3286
July	5.9403	15.237	0.9570	0.3008	5.2214	12.916	0.9573	0.2307
August	5.7908	15.833	0.9391	0.3838	5.0897	13.441	0.9396	0.2940
8-month mean	5.8861	15.230	0.9397	0.4117	5.1724	12.916	0.9402	0.3151

[a]The form of the equation is $t = a \times w + b$, where t is the total channel radiance, w is the filtered window channel radiance, and a and b are the regression coefficients. The linear-correlation coefficients are given by r^2, and the estimated variances are given by σ^2. The coefficients with the subscript *uf* correspond to the unfiltered total, filtered window case, while those with the subscript *ff* correspond to the filtered total, filtered window case.

represented the relationship between the filtered window and filtered (and unfiltered) total channel measurements for each of the eight months from January through August, 1998. The slopes, intercepts, linear-correlation coefficients, and estimated variances are presented in Table 1. The 8-month mean regression fit of the filtered total channel to the filtered window is plotted in Figure 1 as a light gray line. From Figure 1, we can see that the regression fit from Table 1 along with the corresponding 1 σ_{ff} value of 0.5613 Wm^{-2} well represents the observed relationship between the filtered total and filtered window channels. While there is some variance in the monthly regression fits, possibly due to either the seasonal cycle or the 1998 ENSO event [see *Wong et al.*, 2000], the individual fits for each month tended to be fairly similar to one another, with the monthly data sets having a standard deviation about the eight-month mean of 0.0057. Since the functional forms of the regression fits for the first eight months of 1998 are fairly similar, for clarity only the average regression fit has been compared to the corresponding CERES data in Figure 1.

3. Comparison of Theoretical Calculations to Measured Radiances

[8] In order to facilitate a comparison of theory with measurements, we ran our line-by-line models using the *McClatchey et al.* [1972] tropical atmosphere and a variety of DCC parameterizations with cloud tops between 13 and 19 km for the cases considering the CERES window and total channel response functions. The results of the line-by-line calculations are presented along with the regression to the CERES data in Figure 3. The small variance in the line-by-line calculations observed in Figure 3 is associated with different assumptions concerning the DCC optical properties, e.g., the functional form of the extinction coefficients, cloud optical depths, and cloud top altitudes. The various assumptions along with their results can be easily grouped into three broad categories represented in Figure 3 by three different symbols. As illustrated by Figure 3, the results from the theoretical calculations are in good agreement with the CERES measurements. The ratio of the line-by-line calculations to the regression of the measurements is found to have a mean of 1.0148 (i.e., the bias equals 0.0148) and a standard deviation of 0.0022. In comparison, the corresponding standard deviation between the regression fit and the CERES measurements shown in Figure 1 is 0.0173. Thus, by comparing Figures 1 and 3, we see that the results from the line-by-line algorithm fall well within the scatter of the CERES measurements around the regression fit. This suggests that the window channel radiances can be used to accurately simulate the broadband longwave radiances.

[9] Even though the theoretical calculations fall within the envelope defined by the CERES measurements, we found that for brightness temperatures below 215 K the line-by-line calculations tended to exceed the regression fit of the CERES data by ~1.5%. The agreement between theory and measurement can be noticeably improved by focusing upon only those cases which both use the most realistic cirrus cloud extinction coefficients (provided by S. Kato and by R. Arduini, private communications 1998) and have optical paths that average less than one per kilometer

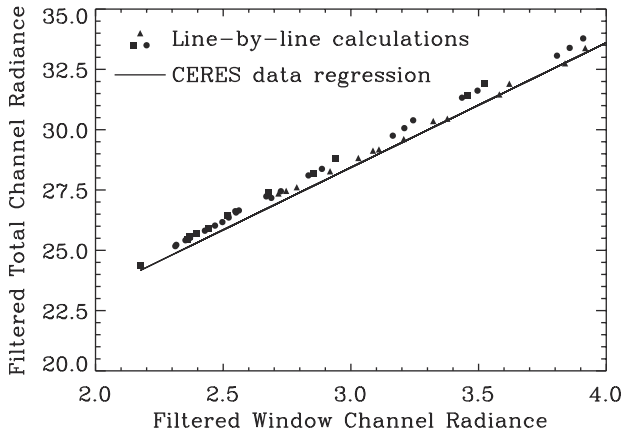

Figure 3. Comparison between the regression fits to the CERES measurements (solid line) and the calculated values from the line-by-line algorithm (filled triangles, circles and squares) for the relationship between the filtered window and filtered total channel radiances (Wm^{-2} sr^{-1}) for the nighttime conditions involving deep convective clouds (DCC). The filled triangles represent non-black cirrus with optical depths less than one per kilometer. The filled circles represent non-black cirrus with optical paths greater than one per kilometer. The filled squares represent blackbody cirrus.

of path length. The non-black cirrus extinction has been applied to an altitude range from 11 kilometers to cloud top, and is applicable to the spectral ranges of both the CERES window and total channels. For these non-black cloud cases, represented in Figure 3 by the filled triangles, the ratios of the line-by-line calculations to the regression of the measurements approach even closer to unity, having a mean of 1.0078 and a standard deviation of 0.0050. Indeed, for the filtered window channel radiances between 2.7 and 4.0 Wm^{-2} sr^{-1}, this subset comprises the values which are found closest to the regression line. In addition, these results compare very favorably with the standard deviation of the regression fit to the CERES measurements (0.0173), and the standard deviation among the individual regression fits for the monthly data sets (0.0057). In contrast, the values that correspond to the line-by-line results that incorporate black clouds, represented in Figure 3 by the filled squares, define the uppermost limit of the filtered window to filtered total channel relationship. Values derived from the line-by-line calculations using non-black extinction coefficients but with average optical paths greater than one per kilometer are represented in Figure 3 by the filled circles and tended to fall between these two extreme cases. To enable future comparisons, we have created regression fits for the calculated filtered window and filtered (and unfiltered) total channel results for the various cirrus cases. The slopes, intercepts, linear-correlation coefficients, and estimated variances are presented in Table 2. In synopsis, the comparison between the line-by-line calculations and the regression fit to the CERES measurements suggests that the DCC systems are best represented when the cirrus clouds are taken to have non-black extinction coefficients with optical paths averaging less than one per kilometer. While our results suggest that non-black cirrus clouds are more representative of the

Table 2. Linear Regressions Similar to Those Presented in Table 1 Except for the Theoretically Calculated CERES Window and Total Channel Radiances[a]

Cloud Case	a_{uf}	b_{uf}	r^2_{uf}	σ^2_{uf}	a_{ff}	b_{ff}	r^2_{ff}	σ^2_{ff}
1	5.6142	16.274	0.9986	0.3069	4.9231	13.917	0.9987	0.2649
2	6.1970	14.846	0.9994	0.1326	5.4267	12.684	0.9995	0.1142
3	6.2943	14.624	0.9994	0.2112	5.5101	12.493	0.9994	0.1825
4	5.9400	15.477	0.9969	0.2147	5.2043	13.229	0.9969	0.1855

[a]The four cloud cases correspond to (1) non-black cirrus with optical depths less than one per kilometer, (2) non-black cirrus with optical paths greater than one per kilometer, (3) blackbody cirrus, and (4) all cirrus cases.

CERES data, for the remainder of this paper we will continue to consider all of our cloud parameter cases.

[10] In addition to the non-black spectral signatures of the DCC systems, there are also some notable absorption and emission features associated with the trace species CO_2, O_3 and H_2O. These spectral signatures are quite evident in Figure 2. Since CO_2, O_3 and H_2O have an impact upon the upwelling TOA radiances, we have examined the impact of varying the abundances of these trace species.

[11] Carbon dioxide possesses a rather strong absorption/emission feature which is located from 600 to 750 cm^{-1}, a spectral range close to the maximum of the Earth's outgoing thermal infrared radiation. This CO_2 spectral feature has a significant effect upon the measured TOA total channel radiances even for the DCC case. In contrast, CO_2 absorption and emission have only a minimal effect upon the outgoing window channel radiances, especially for the DCC case. Since the abundance of CO_2 is known to be slowly increasing with time due to anthropogenic emissions [*Intergovernmental Panel on Climate Change* (*IPCC*), 1995], we ran line-by-line calculations to test the impact of a 10% increase in the CO_2 abundance from 350 ppmv to 385 ppmv. Such an enhancement to the CO_2 abundance results in the ratio of the line-by-line calculations to the regression of the measurements being altered to a mean of 1.0160 and a standard deviation of 0.0022. This is just over a 0.1% change from the reference case; therefore, a 10% increase to the CO_2 abundance has a negligible effect upon the results presented in Figure 3.

[12] Ozone possesses important absorption/emission bands located at 1042 cm^{-1} and 701 cm^{-1}. The 1042 cm^{-1} O_3 band, which is located near the center of the CERES window channel, has a significant impact both upon the window and total channel measured TOA radiances. In contrast, because the significantly weaker 701 cm^{-1} O_3 band is heavily overlapped by the 667 cm^{-1} CO_2 band, the 701 cm^{-1} O_3 band has a more modest impact on the TOA total channel radiance. As with CO_2, human activities are altering the abundance of O_3 in the atmosphere. Indeed, a significant reduction in stratospheric O_3 has been observed in the polar regions, though a more modest reduction in the tropics is suggested by measurements for the stratospheric O_3 [*IPCC*, 1995]. Consequently, we ran line-by-line calculations to test the impact of decreasing the stratospheric O_3 abundance by 10%. Such a reduction in the stratospheric O_3 abundance changes the ratio of the line-by-line calculations to the regression of the measurements to a mean of 1.0163 and a standard deviation of 0.0022. Again, this is just over a 0.1% change from the reference case. Thus, a 10% decrease to the stratospheric O_3 abundance has a negligible effect upon the results presented in Figure 3.

[13] Water vapor, an ubiquitous absorber throughout the thermal infrared, is the principal greenhouse absorber in the Earth's atmosphere [*Inamdar and Ramanathan*, 1994]. Nevertheless, since most of the H_2O absorption occurs in the lower to middle troposphere, we do not anticipate that changes to the H_2O abundance will significantly impact the TOA radiances for the DCC case. To test this assumption, we ran the line-by-line calculations to examine the impact of decreasing the stratospheric H_2O abundance by 10%. We found that such a reduction in the stratospheric H_2O abundance results in the ratio of the line-by-line calculations to the regression of the measurements having a mean of 1.0146 with a the standard deviation 0.0022, values that are virtually the same results as the reference case. Thus, changes to the stratospheric H_2O abundances are not expected to affect the results presented in Figure 3.

4. Derived Nighttime Relationship Between Unfiltered Window and Unfiltered Total Channel Radiances

[14] The discussion has so far focused upon the window and total channel data which incorporate the response functions of the CERES instrument. Studies that investigate climate sensitivity or atmospheric energetics, however, require unfiltered radiances, i.e., radiances that are representative of the energies encountered by the satellite instrument prior to their passage through the optical system. Hence, we have also examined the relationship between the window and total channel data where the effects of the response functions have been removed. A thorough description of the spectral correction method used to remove the response functions from the CERES data has been presented in *Loeb et al.* [2001]. In accordance with CERES protocol, whenever the window channel response function is omitted, the window channel calculations are assigned the spectral range from 848 to 1235 cm^{-1} (8.1 to 11.8 μm). The results of the line-by-line calculations neglecting the window and total channel response functions are presented along with the regression of the unfiltered CERES data in Figure 4. For this case, the ratio of the line-by-line calculations to the regression of the measurements is found to have a mean of 1.0125 and a standard deviation of 0.0022. This result, which can qualitatively be seen by comparing Figure 4 to Figure 3, reveals that the unfiltering process lowers the bias between the theoretical calculations and the CERES data by approximately 0.2%. While the unfiltering process produces only a small change to the bias, there exists the potential that compensating errors may arise from the unfiltering of the window and total channel data. Thus, we separately considered the unfiltering of the window and total channels.

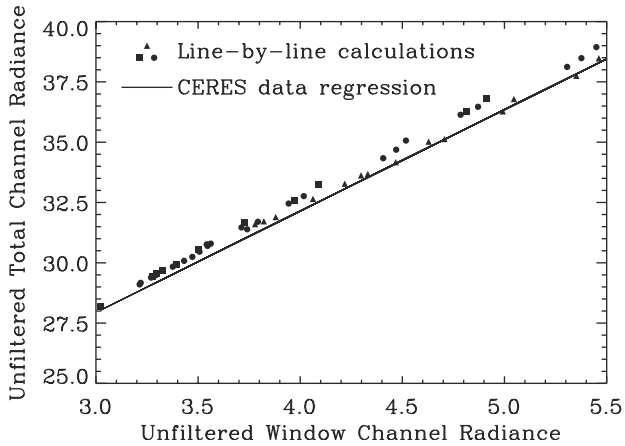

Figure 4. Same as Figure 3 except that the comparison is for the relationship between the unfiltered window and unfiltered total channel radiances (Wm^{-2} sr^{-1}).

[15] The response function for the CERES window channel aboard the TRMM spacecraft is presented in Figure 5 for the wave number range extending from 0 to 2000 cm^{-1}. The design of CERES window channel takes advantage of the spectral range where the reduced molecular absorption in clear sky atmospheres allows a significant fraction of the upwelling radiance emitted from the vicinity of the Earth's surface to escape to space. As can be seen from Figure 5, the window channel response function has a fairly uniform throughput over the designed spectral range and then falls off quickly around the half power points located at 848 and 1235 cm^{-1}. The window channel response function also has additional minor but important semi-transparent spectral regions between 5 and 65 cm^{-1} and between 330 and 420 cm^{-1}. Since our line-by-line model has been formulated to apply the window channel response function to the entire infrared spectral region, 0 to 3000 cm^{-1}, our theoretical calculations can account for the additional radiance measured within these far-infrared spectral regions. We have, however, investigated the impact of neglecting the far-infrared contribution. If we consider window channel response function to be non-zero only for the spectral interval from 835 to 1250 cm^{-1}, we find that the ratio of the line-by-line calculations to the regression of the measurements for the filtered window, filtered total case has a mean of 1.0214 and a standard deviation of 0.0027 while the ratio for the unfiltered window, unfiltered total case has a mean of 1.0191 and a standard deviation of 0.0027. Thus, neglecting the far-infrared contribution to the window channel measurements results in nearly a 0.7% bias as compared with the case when the window radiances are handled correctly. This 0.7% bias is encountered irrespective of whether we are considering the filtered window, filtered total case, or the unfiltered window, unfiltered total case. The reason being that the functional form for both the filtered and unfiltered total channel radiances is given in terms of a linear relationship to the filtered window channel. This emphasizes the importance of accounting for this far-infrared contribution.

[16] Comparing Figures 2 and 5 reveals that for the DCC case the window channel covers a spectral range which is characterized by optically thick blackbody emission. There is also a small contribution due to stratospheric and upper tropospheric ozone, though as previously discussed this has a small impact upon the ratio of the line-by-line calculations to the regression of the satellite measurements. More importantly, however, the window channel response function lies far from the peak of the DCC emission curve, and thus there is little correlation with the response function and the Earth's TOA emitted radiance.

[17] Because of the similarity of the Earth's TOA radiance for the DCC case to blackbody emission, a series of calculations were run to determine the ratio of the unfiltered to filtered window channel radiances for blackbody emission with temperatures ranging from 190K to 290K. The unfiltered to filtered ratio is defined by the expression:

$$\text{ratio} = \frac{\int_{\Delta\omega} B_\omega(T)d\omega}{\int_{\Delta\omega} B_\omega(T)R_\omega d\omega} \tag{2}$$

where $B_\omega(T)$ is the planck function at wave number ω and temperature T, and R_ω is the value of the response function at wave number ω. As illustrated by Figure 6, we found that for temperatures between 190K and 290K the unfiltered to filtered window channel ratio ranges from 1.3880 to 1.4051 with a mean of 1.3992. If the temperatures had been restricted to the range from 235K to 290K, which for the CERES data correspond to clear sky and low to middle cloud conditions that constitute a majority of scene types, then the ratio of the unfiltered to filtered window channel ratio would range from 1.3989 to 1.4050 with a mean of 1.4025. This small variance (±0.2%) about the mean value suggests that a single value for the unfiltering coefficient could be used for most scene types. The advantage of a single unfiltering coefficient is its complete independence from scene dependent details such as scene type and emission temperature. Indeed, for the CERES window channel, an unfiltering coefficient was derived from the calibration data to have a value of 1.4019, which is in good agreement with our analysis. For the DCC case, however, the use of a single unfiltering coefficient could lead to a non-negligible bias; therefore, we have directly applied the results from the line-by-line calculations which explicitly take into consideration the temperature dependence of the

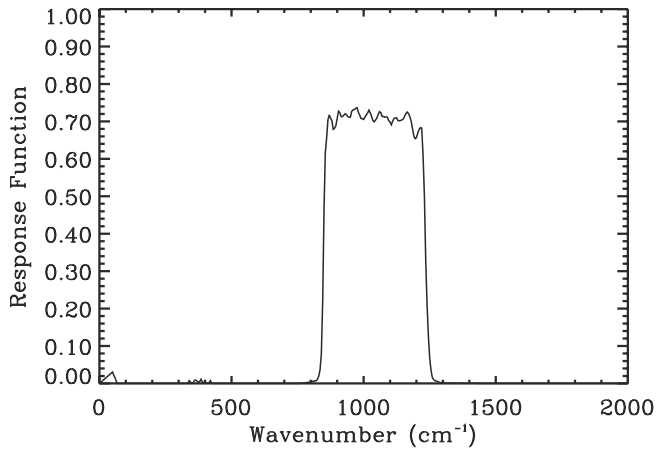

Figure 5. The spectral response function for the CERES/TRMM thermal infrared window channel.

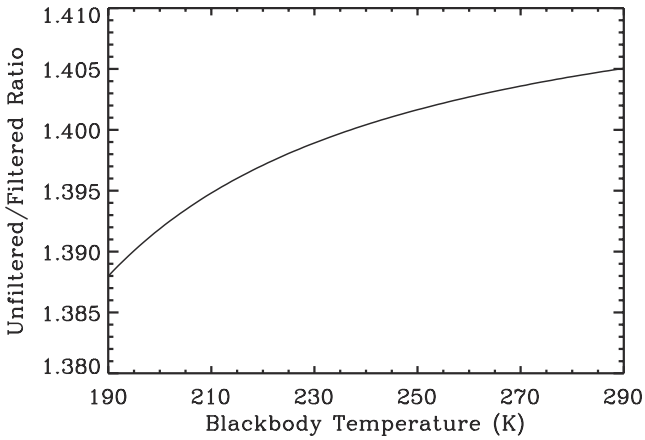

Figure 6. Ratio of unfiltered to filtered radiances for the CERES window channel assuming a blackbody source.

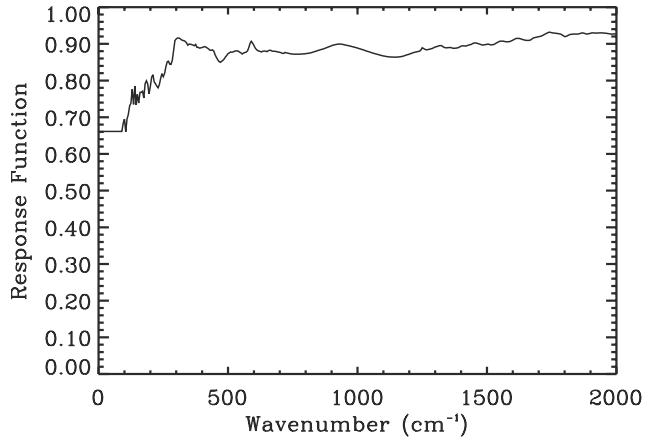

Figure 8. The spectral response function for the thermal infrared region of the CERES/TRMM total channel.

unfiltering coefficient. A comparison of the unfiltered window to filtered total channel relationship for the line-by-line calculations to the regression of the CERES data are presented in Figure 7. Comparing the unfiltered window, filtered total case in Figure 7 to the filtered window, filtered total case in Figure 3 demonstrates that the unfiltering of the window channel is not a significant source of error.

[18] The CERES total channel was designed to measure the entire range of solar reflected and thermal infrared emitted energies from the Earth. Since our study focuses upon the intercomparison of the window and total channel measurements for nighttime conditions, only the thermal infrared portion of the spectrum needs be considered here. Figure 8 illustrates the total channel response function for the wave number range from 0 to 2000 cm^{-1}. Ideally, the total channel response function should be uniformly transmissive throughout the entire range of solar and thermal emitted radiation, and indeed, for much of the spectral range from 300 to 25,000 cm^{-1} the total channel response function is relatively uniform [*Lee et al.*, 1998; *Priestley et al.*, 1998]. In contrast, for the far-infrared, wave numbers less than 300 cm^{-1}, there appears to be a non-negligible reduction in the throughput of the total channel. For conditions which are representative of clear skies or low cloudiness, the middle to middle far-infrared, 400 to 1250 cm^{-1}, contributes a very large fraction of the total energy; therefore, the observed decrease in the far-infrared throughput is not critical. For the DCC case, however, the peak of the emission curve shifts toward the far-infrared and the importance of that region is greatly magnified. Indeed, a comparison of Figures 2 and 8 emphasizes that the peak of emission curves for DCC are located near the spectral range where the total channel becomes less transparent. This suggests that there may be a functional relationship between the unfiltering of the total channel and the effective emission temperature.

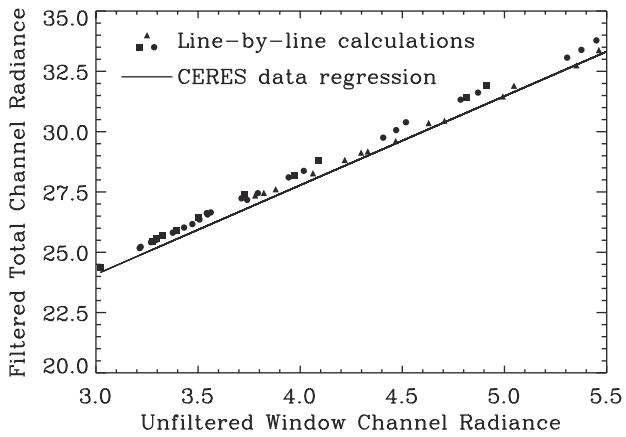

Figure 7. Same as Figure 3 except that the comparison is for the relationship between the unfiltered window and filtered total channel radiances (Wm^{-2} sr^{-1}).

[19] The far-infrared portion of the total channel response function, however, is more difficult to characterize than the remainder of the infrared and visible portions of the spectrum. In order to test the uncertainty of the total channel response function in the far-infrared, we reran the line-by-line calculations assuming that the total channel response function has a constant value of 0.81 for wave numbers <350 cm^{-1}. Such a prescription is not arbitrary since the modified response function yields the same integrated input as that obtained using the values illustrated in Figure 8. The results of the line-by-line calculations using the modified total channel response function are presented in Figure 9 and yield a ratio of the line-by-line calculations to the regression of the measurements which have a mean of 1.0128 and a standard deviation of 0.0021. This is less than a 0.2% change from the reference case; therefore, the uncertainty in the far-infrared portion of the total channel response function does not drastically change the results that have been presented in Figure 3.

[20] As with the window channel, we have run a series of calculations to determine the ratio of the unfiltered to filtered total channel radiance for blackbody emission with temperatures ranging from 190K to 290K. For this range of temperatures, we have found that the unfiltered to filtered total channel ratios range from 1.1595 to 1.1409. This modest functional dependence, as illustrated in Figure 10, demonstrates that a single value for the unfiltering ratio is not appropriate for the entire range of temperatures. Additional calculations based upon a formulation provided by Y. Hu (private communications, 1998), and upon the MOD-

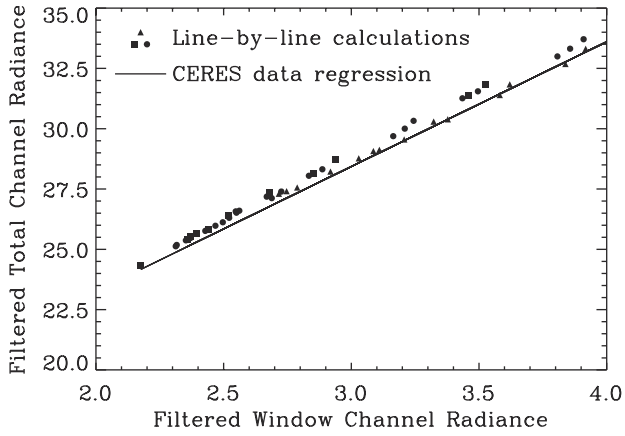

Figure 9. Same as Figure 3 except that the comparison for the relationship between the filtered window and filtered total channel radiances (Wm^{-2} sr^{-1}) takes the filtered total response function to have a value of 0.81 for wave numbers less than 350 cm^{-1}.

TRAN code provided by F. Rose (private communications, 1998) agree very well with our calculations. To facilitate a comparison of the results from Figure 10, for the total channel, to the results from Figure 6, for the window channel, we have taken both of these figures to have approximately the same range, 2.2%, along the vertical axis for the ratios of the unfiltered to filtered radiances. Figures 6 and 10 illustrate that the magnitudes of the temperature dependence of the window and total channels are similar although the direction of their dependence is reversed. Despite the observed temperature dependence, an unfiltering coefficient of 1.143 appears to be a reasonably good approximation (±0.2%) for the temperature range from 260K to 290K, which is representative of tropical clear sky and boundary layer stratus cloud conditions. In contrast, the use of this single unfiltering coefficient could lead to a non-negligible bias for the DCC case, especially considering that the unfiltering coefficients, as illustrated by Figure 10, span the range from 1.153 to 1.159 for temperatures between 190K and 215K. Thus, we have explicitly taken into consideration the temperature dependence of the unfiltering coefficients when applying the CERES unfiltering relationship to the total channel. Our results are presented in Figure 11. Since a single unfiltering coefficient is insufficient, *Loeb et al.* [2001] have developed a more precise regression formula to determine the unfiltered longwave nighttime radiance from the filtered window and filtered total channel radiances. The *Loeb et al.* [2001] regression formula yields far higher accuracies than possible with a single unfiltering coefficient, and has therefore been implemented into the CERES data processing algorithms.

[21] Comparing the filtered window, unfiltered total case in Figure 11 to the filtered window, filtered total case Figure 3 clearly demonstrates that the unfiltering of the total channel does not introduce a significant error. There remains, however, an unexplained discrepancy with the line-by-line calculations producing an ∼0.8% to ∼1.5% overestimation of the regression fits to the functional relationship between the CERES total and window channels. While our investigation of the uncertainties in the far-infrared portion of the total channel response function have yet to uncover any problems, the lack of measurements for the far-infrared portion of the CERES total channel response function does emphasize the need to accurately measure instrument response functions into the far-infrared. Moreover, despite recent advances in our knowledge of the far-infrared water vapor absorption [*Tobin et al.*, 1999], there remains significant uncertainties with regards to the strengths of the spectroscopic features in the pure-rotation band of water vapor [*Rothman et al.*, 1998]. Such uncertainties have the potential to manifest themselves as discrepancies between theory and measurements. Thus, additional spectral measurements of the far-infrared are needed to improve our understanding of the far-infrared radiative effects of both water vapor absorption and the scattering and absorption by cirrus.

[22] To further complicate matters, the tropical mean (*TM*) yields a CERES total channel nighttime measurement which is about 1.5% higher than the equivalent nighttime measurement from the Earth Radiation Budget Satellite (ERBS) scanner taken during the 1985 to 1989 time frame [see *Wielicki et al.*, 1999]. The source of this discrepancy may well come from the CERES or ERBS instruments or

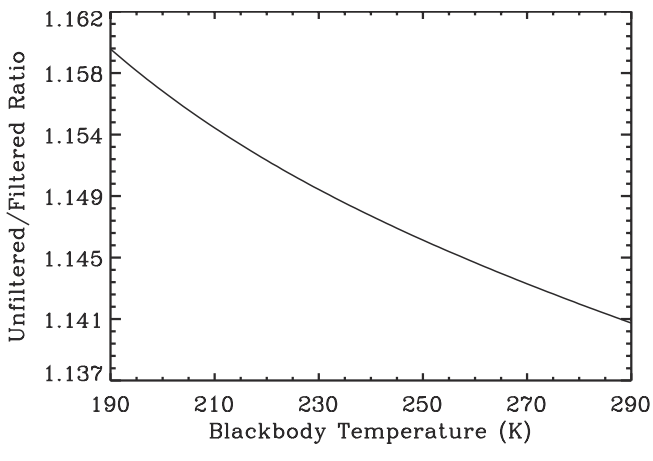

Figure 10. Ratio of unfiltered to filtered radiances for the CERES total channel assuming a blackbody source.

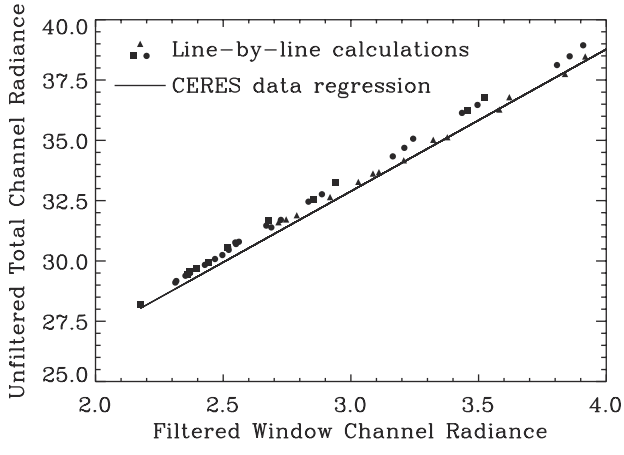

Figure 11. Same as Figure 3 except that the comparison is for the relationship between the filtered window and unfiltered total channel radiances (Wm^{-2} sr^{-1}).

actual changes in the radiative state of the tropics. While the calibration of the CERES instrument is almost certainly better than the ERBS instrument, if this discrepancy arises from the CERES instrument, then the accepted CERES total channel response function is too low, meaning that the measured values are increased too much during unfiltering. Our comparison between theory and measurements for the DCC case, however, suggests that the CERES total channel response function is too high for the far-infrared. Consequently, the discrepancy in the *TM* suggests that the CERES total channel response function may be too low in the near to mid-infrared portion of the spectrum. The results from the DCC and *TM* cases, therefore, provide insight for two totally different spectral regions of the CERES total channel response function.

5. Three Channel Intercomparison

[23] Obtaining a statistically robust relationship between the infrared window channel and the broadband total channel allows for studies to be conducted which assess the relative consistency between the shortwave channel and shortwave portion of the total channel. Since these studies rely upon the inherent redundancy in the three CERES channels we refer to this method as the three channel intercomparison. Assuming that an appropriate technique can be developed which will convert the 835 to 1250 cm^{-1} infrared window channel into a "synthetic" broadband infrared channel (i.e., 100 to 2000 cm^{-1}), shortwave radiances can then be determined using either the shortwave channel, or by differencing the "synthetic" broadband infrared and total channels. Similarly, the broadband infrared radiance can be determined by subtracting the shortwave channel from the total channel, and the total radiance can then be calculated by summing the shortwave and "synthetic" broadband infrared channel.

[24] The process of converting the infrared window radiances into "synthetic" broadband infrared radiances is accomplished by regressing the nighttime infrared window channel measurements against the nighttime total channel broadband radiance for the same tropical DCC footprints. We have limited this analysis to tropical (±20° latitude) nadir footprints comprised entirely of DCC systems whose brightness temperatures are less than 215 K and whose spatial extent is at least 40 km in the satellite ground track direction. The 40 km or greater spatial extent for the DCC systems was established by requiring that a minimum of 2 consecutive nadir window channel brightness temperature measurements were below the threshold value of 215 K. Since DCC's exist only at high altitudes (>10 km) we have minimized uncertainties due to atmospheric scattering and water vapor absorption, and the resulting relationship is statistically robust as seen in Figure 1. Daytime longwave radiance measurements for DCC's are then obtained both by applying the conversion technique to the infrared window channel measurements and by subtracting shortwave channel measurements from total channel measurements. By regressing the difference of these two daytime longwave radiance values against the daytime filtered shortwave measurements, both inconsistencies (biases) and changes (trends) in the relationship between the estimated spectral response functions of the shortwave channel and shortwave portion of the total channel can be seen. Because DCC's occur in approximately 1% of all nadir measurements, these calculations are performed on a monthly basis in order to obtain a statistically rigorous sample size.

[25] Since the spectral weighting of solar energy reflected by the DCC's is a weak function of solar zenith angle, uncertainties in the unfiltering algorithm for the shortwave radiances are minimized. *Loeb et al.* [2001] demonstrated that errors introduced by the unfiltering algorithms for the shortwave channel are less than 0.2%. We have implicitly assumed in this study that the emitted longwave radiance is independent of solar zenith angle and that the algorithms used in determining the spectral unfiltering coefficients are applied consistently to both the shortwave channel and shortwave portion of the total channel. Thus, any inconsistencies uncovered which exceed the known uncertainties in the unfiltering algorithms are most likely due to our estimate of the spectral response functions.

[26] *Priestley et al.* [2000] have demonstrated that the three channel intercomparison technique empirically assesses the relationship between the true spectral response functions of the shortwave portion of the shortwave and total channels and that our best estimates of these functions is determined during the radiometric ground calibrations. This method does not assess the absolute accuracy of either channel. Any disagreement between truth and estimate may be quantified by

$$\text{error} = \frac{-\left(d\Delta/dI_f^{sw}\right) \times 100}{\hat{a}^{lw/tot}\left(\hat{a}^{sw}/\hat{a}^{sw/tot}\right)} \tag{3}$$

where Δ is the daytime longwave difference, I_f^{sw} is the daytime filtered shortwave measurement, and $\hat{a}^{sw}$, $\hat{a}^{sw/tot}$ and $\hat{a}^{lw/tot}$ are our estimates of the true spectral unfiltering coefficients a^{sw}, $a^{sw/tot}$ and $a^{lw/tot}$. Solving the denominator in Equation 3 yields a value of 1.12 for DCC. A negative error from Equation 3 would imply that either the estimated spectral response function for the shortwave channel, $\hat{S}_\lambda^{sw}$ is low, or the estimated spectral response function for the shortwave portion of the total channel, $\hat{S}_\lambda^{sw/tot}$ is high. A positive error would imply the opposite. Since the shortwave CERES data products are derived from shortwave channel measurements only, errors in $\hat{S}_\lambda^{sw/tot}$ will not affect these products. We have no indication from this validation test whether $\hat{S}_\lambda^{sw}$ or $\hat{S}_\lambda^{sw/tot}$ is incorrect. Moreover, even if we knew which estimate was in error, there is no information of the error as a function of λ since our tests were on the integrals of S_λ over λ. What our study does provide is a direction in which to proceed as one reviews all of the ground based radiometric calibration/characterization data to look for possible experimental/algorithm errors.

[27] In the CERES/TRMM Edition-1 ERBE-like data products, the three-channel intercomparison revealed an unvarying bias of 0.9% between the shortwave and shortwave portions of the total channel over the eight month data set. Upon extensive review of the algorithms used to analyze data collected during the ground radiometric calibration/characterization testing, small but significant errors were found and corrected in the derivation of the spectral response functions above 2.0×10^4 cm^{-1} (i.e., below 0.5 μm). These new spectral response functions were then implemented in

the CERES/TRMM Edition-2 ERBE-like data products. The new response functions produce unfiltering coefficients which increase the calculated unfiltered radiance between 5.0×10^3 and 3.3×10^4 cm^{-1} (0.3 and 2.0 μm) by 0.16% for the shortwave channel and decrease the calculated unfiltered radiance by 0.65% for the total channel between 5.0×10^3 and 3.3×10^4 cm^{-1} for a 5800K blackbody emission spectrum. Results of applying the three-channel intercomparison analyses to the Edition-2 data products yield inconsistencies of less than 0.2% on average over the eight month data set. Statistically, the three-channel intercomparison is not sufficiently strong to allow us to say that these remaining inconsistencies are significant.

[28] In summary, the vicarious three-channel study was successful in directing the instrument working group where possible errors may have occurred during the derivation of the spectral response functions. At the same time, the final resulting response functions were not tuned via the three-channel vicarious study such that the resulting inconsistencies were driven to a null value. All implemented changes are the result of small but significant physically traceable errors in the original effort. Vicarious studies provide valuable ancillary data sources which must be taken into account before the physical processes occurring in an instrument can be fully understood.

[29] Another approach to analyzing the daytime measurements considers the case of all-sky data and thus provides more comprehensive results. This approach relies upon the tropical mean (*TM*), which is the average of the all-sky broadband longwave nadir data taken over the ocean in the tropics. Again, for present purposes the tropics have been defined to be ±20° latitude. Our analysis has demonstrated that the *TM* is relatively constant with monthly values of the *TM* having a one sigma variance of order 0.5%. We have determined the day-night differences (*DN*) for the tropical mean:

$$DN = TM(day) - TM(night) \quad (4)$$

using the broadband longwave values derived both from the CERES window channel radiances and from differencing the CERES shortwave and total channels. The *DN* for the broadband longwave radiances derived from the CERES window channel is of order 1 Wm^{-2} sr^{-1} and tends to be insensitive to the regression, gain error, or offset error. In contrast, the *DN* for the broadband longwave radiances derived from the CERES/TRMM Edition-1 shortwave and total channel data implies a CERES shortwave inconsistency of 1.2%. Either the shortwave radiance is 1.2% low or the shortwave portion of the total channel is 1.2% high. This study using all-sky agrees with our three channel analysis of deep convective clouds since they both show about a 1% shortwave inconsistency.

6. Conclusions

[30] A highly correlated linear relationship between the CERES window and total channel measurements exists for nighttime conditions corresponding to deep convective clouds. This relationship which was derived from measurements is consistent with theoretical line-by-line calculations to ~1.5%. If realistic extinction coefficients and cirrus cloud optical paths less than one per kilometer are used, the differences between the theoretical calculations and the regression fit to the measurements is nearly halved. Investigations are still underway to fully capture the sources of the remaining differences between the line-by-line results and the regression to the CERES measurements.

[31] Comparing the various combinations of the CERES window and total channels, with and without the response functions included, clearly demonstrates that the unfiltering of these channels does not introduce a significant source of error.

[32] The broadband longwave values as derived from the CERES window channel and as derived by differencing the CERES shortwave and total channels are consistent to about 1%. Our investigation suggests that the small remaining residual is due to our uncertainty in the spectral response functions of either the shortwave channel or the shortwave portion of the total channel.

[33] **Acknowledgments.** The authors would like to acknowledge the technical advice of B. A. Wielicki and G. G. Gibson concerning the preparation of this manuscript. This research was supported through funding from the NASA Earth Science Enterprise Program.

References

Barkstrom, B. R., The Earth Radiation Budget Experiment (ERBE), *Bull. Am. Meteorol. Soc.*, *65*, 1170–1185, 1984.

Barkstrom, B. R., and G. L. Smith, The Earth Radiation Budget Experiment: Science and implementation, *Rev. Geophys.*, *24*, 379–390, 1986.

Clough, S. A., and M. J. Iacono, Line-by-line calculation of atmospheric fluxes and cooling rates, 2, Application to carbon dioxide, ozone, methane, nitrous oxide, and the halocarbons, *J. Geophys. Res.*, *100*, 16,519–16,535, 1995.

Clough, S. A., F. X. Kneizys, and R. W. Davies, Line shape and the water vapor continuum, *Atmos. Res.*, *23*, 229–241, 1989.

Clough, S. A., M. J. Iacono, and J.-L. Moncet, Line-by-line calculations of atmospheric fluxes and cooling rates: Application to water vapor, *J. Geophys. Res.*, *97*, 15,761–15,785, 1992.

Duvel, J.-P., and P. Raberanto, A geophysical cross-calibration approach for broadband channels: Application to the ScaReB experiment, *J. Atmos. Oceanic. Technol.*, *17*, 1609–1617, 2000.

Ellingson, R. G., and Y. Fouquart, The intercomparison of radiation code in climate models: An overview, *J. Geophys. Res.*, *96*, 8925–8927, 1991.

Inamdar, A. K., and V. Ramanathan, Physics of greenhouse effect and convection in warm oceans, *J. Clim.*, *7*, 715–731, 1994.

Intergovernmental Panel on Climate Change (IPCC), *Climate Change, 1994: Radiative Forcing of Climate Change and an Evaluation of the IPCC IS92 Emission Scenarios*, 339 pp., Cambridge Univ. Press, New York, 1995.

Kratz, D. P., and F. G. Rose, Accounting for molecular absorption within the spectral range of the CERES window channel, *J. Quant. Spectrosc. Radiat. Transfer*, *61*, 83–95, 1999.

Lee, R. B., III, et al., Prelaunch calibrations of the Clouds and the Earth's Radiant Energy System (CERES) Tropical Rainfall Measuring Mission and Earth Observing System Morning (EOS-AM1) spacecraft thermistor bolometer sensors, *IEEE Trans. Geosci. Remote Sens.*, *36*, 1173–1185, 1998.

Loeb, N. G., K. J. Priestley, D. P. Kratz, E. B. Geier, R. N. Green, B. A. Wielicki, P. O'Rawe-Hinton, and S. K. Nolan, Determination of unfiltered radiances from the Clouds and the Earth's Radiant Energy System (CERES) instrument, *J. Appl. Meteorol.*, *40*, 822–835, 2001.

McClatchey, R. A., R. W. Fenn, J. E. Selby, F. E. Volz, and J. S. Garing, *Optical Properties of the Atmosphere*, 3rd ed., 103 pp., Air Force Cambridge Res. Lab., Bedford, Mass., 1972.

Minnis, P., D. F. Young, and E. F. Harrison, Examination of the relationship between outgoing infrared window and total longwave fluxes using satellite data, *J. Clim.*, *4*, 1114–1133, 1991.

Minnis, P., K.-N. Liou, and Y. Takano, Inference of cirrus cloud properties using satellite-observed visible and infrared radiances, Part I, Parameterization of radiance fields, *J. Atmos. Sci.*, *50*, 1279–1304, 1993.

Prabhakara, C., D. P. Kratz, J.-M. Yoo, G. Dalu, and A. Vernekar, Optically thin cirrus clouds: Radiative impact on the warmpool, *J. Quant. Spectrosc. Radiat. Transfer*, *49*, 467–483, 1993.

Priestley, K. J., B. R. Barkstrom, H. C. Bitting, R. B. Lee III, D. K. Pandey, S. Thomas, and K. L. Thornhill, End-to-end spectral characterization of the Clouds and the Earth's Radiant Energy System (CERES) thermistor bolometer, *Proc. SPIE Int. Soc. Opt. Eng.*, *3498*, 12–22, 1998.

Priestley, K. J., B. R. Barkstrom, R. B. Lee III, R. N. Green, S. Thomas, R. S. Wilson, P. L. Spence, J. Paden, D. K. Pandey, and A. Al-Hajjah, Postlaunch radiometric validation of the Clouds and the Earth's Radiant Energy System (CERES) Proto-Flight Model on the Tropical Rainfall Measuring Mission (TRMM) spacecraft through 1999, *J. Appl. Meteorol.*, *39*, 2249–2258, 2000.

Rothman, L. S., et al., The HITRAN molecular spectroscopic database and HAWKS (HITRAN Atmospheric Workstation): 1996 edition, *J. Quant. Spectrosc. Radiat. Transfer*, *60*, 665–710, 1998.

Smith, W. L., H. E. Revercomb, R. O. Knuteson, F. A. Best, R. Dedecker, H. B. Howell, and H. M. Woolf, Cirrus cloud properties derived from high spectral resolution infrared spectrometry during FIRE II, Part I, The high resolution interferometer sounder (HIS) systems, *J. Atmos. Sci.*, *52*, 4238–4245, 1995.

Tobin, D. C., et al., Downwelling spectral radiance observations at the SHEBA ice station: Water vapor continuum measurements from 17 to 26 μm, *J. Geophys. Res.*, *104*, 2081–2092, 1999.

Wielicki, B. A., B. R. Barkstrom, E. F. Harrison, R. B. Lee III, G. L. Smith, and J. E. Cooper, Clouds and the Earth's Radiant Energy System (CERES): An Earth Observing System experiment, *Bull. Am. Meteorol. Soc.*, *77*, 853–868, 1996.

Wielicki, B. A., T. Wong, D. F. Young, B. R. Barkstrom, R. B. Lee III, and M. Haeffelin, Differences between ERBE and CERES tropical mean fluxes: ENSO climate change or calibration, *Tenth Conference on Atmospheric Radiation, Madison, Wisconsin*, June 28–July 2, 1999.

Wong, T., D. F. Young, M. Haeffelin, and S. Weckmann, Validation of the CERES/TRMM ERBE-like monthly mean clear-sky longwave dataset and the effects of the 1998 ENSO event, *J. Clim.*, *13*, 4256–4267, 2000.

R. N. Green, D. P. Kratz, and K. J. Priestley, Atmospheric Sciences, NASA Langley Research Center, Hampton, Virginia 23681-2199, USA. (r.n.green@larc.nasa.gov; d.p.kratz@larc.nasa.gov; k.j.priestley@larc.nasa.gov)